PNAS RESEARCH ARTICLE | CHEMISTRY

Contact between water vapor and silicate surface causes abiotic formation of reactive oxygen species in an anoxic atmosphere

Yu Xia[a,b,c], Juan Li[b,d], Yuanzheng Zhang[d], Yongguang Yin[e], Bolei Chen[a,b,e,1], Yong Liang[a,b,1], Guibin Jiang[e], and Richard N. Zare[c,1]

Contributed by Richard N. Zare; received February 4, 2023; accepted June 10, 2023; reviewed by Ariel D. Anbar and Zhong L. Wang

Spontaneous generation of reactive oxygen species (ROS) in aqueous microdroplets or at a water vapor–silicate interface is a new source of redox chemistry. However, such generation occurs with difficulty in liquid water having a large ionic strength. We report that ROS is spontaneously produced when water vapor contacts hydrogen-bonded hydroxyl groups on a silicate surface. The evolution of hydrogen-bonded species such as hydroxyl groups was investigated by using two-dimensional, time-resolved FT-IR spectroscopy. The participation of water vapor in ROS generation is confirmed by investigating the reaction of D_2O vapor and hydroxyl groups on a silicate surface. We propose a reaction pathway for ROS generation based on the change of the hydrogen-bonding network and corresponding electron transfer onto the silicate surface in the water vapor–solid contact process. Our observations suggest that ROS production from water vapor–silicate contact electrification could have contributed to oxidation during the Archean Eon before the Great Oxidation Event.

contact electrification | water vapor–solid interface | hydroxyl radical | hydrogen peroxide | reactive oxygen species

Significance

The origin of atmospheric oxidation is important for understanding the evolution of Earth's early environment and the origin of life. The formation of oxygen species has long been linked to photosynthesis by cyanobacteria. Previous studies demonstrated that contact electrification between liquid water and solids causes the generation of hydroxyl radicals. However, the contribution of this phenomenon to atmospheric oxidation is open to question because the formation of oxygen species at a liquid water–solid interface is affected by the ionic strength of water. This study shows that reactive oxygen species can arise from contact electrification of water vapor with silicate, which may have contributed to oxidation during the Archean Eon.

Hydrogen peroxide (H_2O_2), as one of the reactive oxygen species, is a simple but important compound in nature because it plays key roles in many aspects ranging from environmental chemistry (1), biochemistry (2, 3), and geoscience to human health (4). Intriguing hypotheses proposed that H_2O_2 once acted as a transitional electron donor prior to H_2O for the origin of life (5) and evolution of oxygenic photosynthesis (6–8) on Earth (8, 9) because water can only provide electrons with the help of chlorophyll-*a* and the water-oxidizing complex. Although it is generally thought that oxidative photosynthesis also existed prior to the Great Oxidation Event, it has been proposed that H_2O_2 made a significant contribution to Archean atmospheric oxygenation and may create evolutionary pressure that forced existing photoautotrophs to adapt to locally oxidized environments (6, 8–11). This issue is complicated by the fact that various abiotic geochemical sources of H_2O_2 existed on early Earth (12, 13). Early works reported that the abiotic sources of H_2O_2 may have come from the photolysis of H_2O in the early stratosphere and that H_2O_2 generated in the stratosphere may reach the ground through precipitation (14). However, several theoretical calculations suggest that the amount of H_2O_2 that could reach the ground with precipitation is low owing to the short lifetime of H_2O_2 in the stratosphere (15, 16). Additionally, the fainter Sun during the Archean Eon, with 25 to 30% lower solar luminosity (12), may also reduce the H_2O_2 generation reaction level through the photochemical pathway. In addition, higher UV fluxes from the young sun could cause the decomposition of H_2O_2 in the lower atmosphere. Recent works by Zare and coworkers reported that H_2O_2 is generated spontaneously in aqueous microdroplets (17–22). They also provided evidence that H_2O_2 in the microdroplets was formed without the adsorption of ozone (23). These results indicate that there may be unrecognized pathways for H_2O_2 generation from water. A more recent hypothesis is that H_2O_2 may form at the mineral–water interface along the silicate intertidal zone in lakes, rivers, and oceans on early Earth (8). He et al. conjectured that the mechanism of H_2O_2 generation could be attributed to reactions between water and the surface-bound radicals on silicate minerals (8). It is no coincidence that a recently published study also reported the generation of H_2O_2 from the hydroxyl group on the solid surface and it was suggested that this phenomenon can be attributed to water–solid contact electrification (24). Recently, it was proposed that stress-induced and fracture-induced reactions at silicate surfaces in contact with liquid water could be a source of H_2O_2 to Earth's early atmosphere (10). However, the generation of H_2O_2 at the water–solid interface is dramatically reduced by an increase in the ionic strength of water and H_2O_2 can be hardly detected when the ion concentration is higher than 10^{-5} M (17, 24). We propose that the increase of ion concentration changes the structure of the electrical double layer, thus affecting the electron transfer and the corresponding H_2O_2 generation at the water–solid interface including other reactive oxygen species. Considering

Author contributions: Y.X., B.C., Y.L., and G.J. designed research; Y.X., J.L., Y.Z., Y.Y., B.C., Y.L., and G.J. performed research; Y.X., B.C., Y.L., G.J., and R.N.Z. analyzed data; and Y.X., B.C., and R.N.Z. wrote the paper.

Reviewers: A.D.A., Arizona State University; and Z.L.W., Georgia Institute of Technology.

The authors declare no competing interest.

[1]To whom correspondence may be addressed. Email: bl_chen@jhun.edu.cn, ly76@263.net, or zare@stanford.edu.

This article contains supporting information online at https://www.pnas.org/lookup/suppl/doi:10.1073/pnas.2302014120/-/DCSupplemental.

Published July 17, 2023.

the hypothesis that liquid water on the early Earth came from the universal deluge, the ionic strength of surface water in Archean Eon may have had an ionic strength much higher than 10^{-5} M (note that the ionic strength of rainwater is of order 10^{-3} M) (25, 26). Surface water with kinds of ions reduced the likelihood of H_2O_2 generation at the solid–liquid interface. Therefore, we hypothesize that another pathway that is independent of ionic strength may have contributed to H_2O_2 generation from water. Because we do not know how to quantify the production of ROS from such interactions, it remains only speculative how much this may have contributed to the Earth's early atmosphere. Without doubt, however, this process does represent a new chemical transformation of water into ROS.

Water vapor is the main form of water in the atmosphere. As surface water evaporates, water molecules rise into the atmosphere, leaving most of the ions in the source water. Importantly, unlike water–solid contact electrification is a physicochemical process involving both electrons and ions (27–29), the type of charge transfer in gas–solid contact electrification is electrons (30, 31). Moreover, contact electrification, or frictional charging between gas and solid, is ubiquitous in nature (32). This effect is evident in the atmosphere, which is far from being a pure homogeneous gas. As the troposphere moves, the contact occurs between water vapor and aerosol particles. The water vapor and airborne particulate matter become electrified in friction and collisions with each other. In addition, our previous studies have confirmed that contact electrification can cause spontaneous ROS generation at room temperature (17, 18). The typical temperature range of the Archean Earth (0 to 40 °C) (33, 34) meets the temperature requirements of this process, which further increase the possibility of water vapor participating in the interfacial redox reactions (10, 12, 33, 34). However, the physicochemical processes that accompany the water vapor–solid contact electrification are poorly understood. Therefore, it is crucial to find out what interfacial redox reactions happen when water vapor contacts a solid substrate.

Results and Discussion

Construction of an Ideal Water Vapor–Solid Interface. Our previous work has confirmed that water–solid contact electrification can cause ROS generation on various substrates including carbon powders, oxides, standard soil, and atmospheric fine particles (24). Therefore, building our model based on a solid material with relatively stable chemical properties can eliminate the interference of potential catalytic reactions in our study. Additionally, considering that sandstones are the most abundant weathering end-product minerals in terrestrial environments (35), we set up the ideal water vapor–solid interface based on SiO_2 nanoparticles. Notably, nanoparticles are used to construct large surface areas in the hope of producing physicochemical phenomena strong enough for subsequent detection. *SI Appendix*, Fig. S1 displays the schematic of the experimental setup. Argon gas was first bubbled through water to produce water vapor. The water was deionized (DI) reagent-grade with a resistivity larger than 18 MΩ cm. Argon gas also provides an anoxic atmosphere in the sealed chamber. The humidified Argon gas was then injected into a sealed chamber that is filled with SiO_2 nanoparticles to construct an ideal water gas–solid contact model (Fig. 1*A*). Thus, this model can simulate the water vapor–solid contact and corresponding physicochemical processes in an anoxic atmospheric environment.

Generation of H_2O_2 and Other ROS at the Water Vapor–Solid Interface. As a proof-of-concept experiment, we compared the concentration of ROS between the injected and exiting gas. The

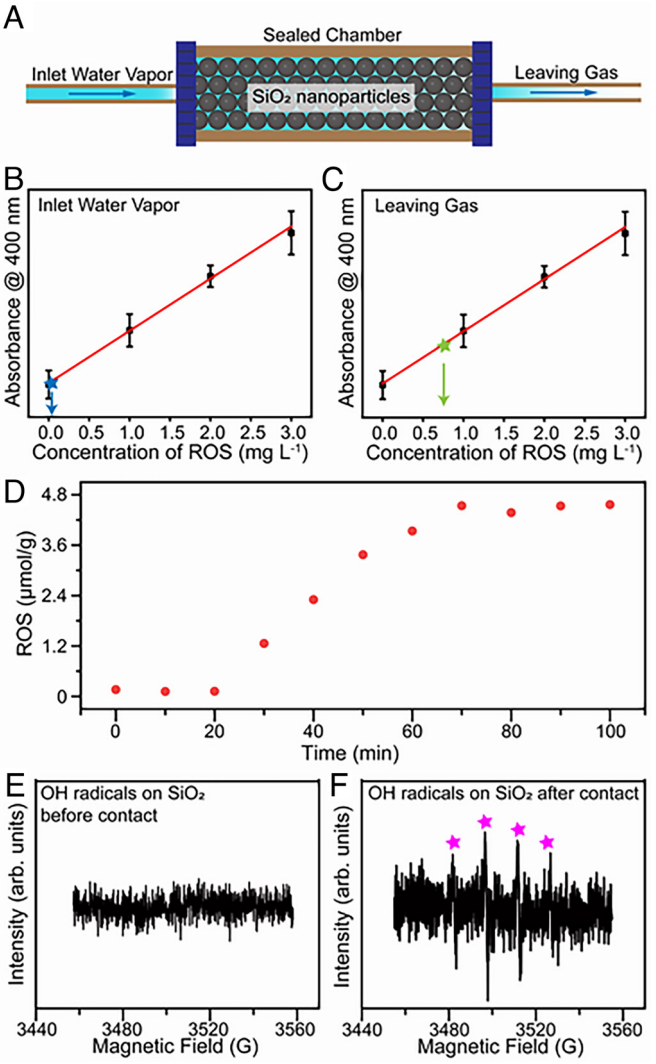

Fig. 1. Generation of ROS during the contact between water vapor and SiO_2 nanoparticles. (*A*) Schematic image of the experimental setup of water vapor–solid interface in a sealed chamber. (*B*) The ROS concentration at the inlet of the sealed chamber. (*C*) The ROS concentration in the leaving gas after the contact between water vapor and SiO_2 nanoparticles. (*D*) The relationship between ROS concentration at the surface of SiO_2 nanoparticles and reaction time during the contact process. (*E*) The ESR spectrum of hydroxyl radicals at SiO_2 nanoparticles before contact occurred. (*F*) The corresponding ESR spectrum of hydroxyl radicals at SiO_2 nanoparticles after contact occurred.

gases were collected by DI water, and they were subsequently mixed with potassium titanium oxalate (PTO, $K_2TiO[C_2O_4]_2 \cdot H_2O$) solutions in equal volume. In previous reports (17, 18, 24), PTO solutions were commonly employed for quantifying H_2O_2 concentrations. However, our DFT calculations (*SI Appendix*, Fig. S2) revealed that PTO reacts not only with H_2O_2 but also with other reactive oxygen species, such as hydroxyl radicals. Distinct differences among DI water, 1.5 ppm H_2O_2 solution, and collected samples can be observed in their mass spectra (*SI Appendix*, Fig. S3*A*). As H_2O_2 is a neutral uncharged species, its signal is undetectable by mass spectrometry; however, the collected sample exhibits a clear signal at *m/z* 36, attributable to hydrated hydroxyl radicals (36). As shown in *SI Appendix*, Fig. S3*B*, both H_2O_2 solution and collected samples can react with PTO, which is consistent with the DFT results. To further verify the *m/z* 36 signal's association with hydroxyl radicals, 1.5 ppm H_2O_2 standard solution was characterized using mass spectrometry in NanoESI mode, while exciting 340 nm UV light during injection

(*SI Appendix*, Fig. S4). The *m/z* 36 signal significantly increased with irradiation, consistent with the fact that UV light excitation can convert H_2O_2 into hydroxyl radicals.

ROS (H_2O_2 and H_2O ·OH) can be detected at a very low level in the injected gas (Fig. 1*B*). The concentration of ROS in the collected solution reached 0.75 mg/mL after 90 min of continuous exiting gas infusion (Fig. 1*C*). This result indicates that ROS formed when contact occurred between water vapor and SiO_2 nanoparticles. The ROS detected in the exiting gas is transported by the carrier gas from the contact process. To further understand the phenomenon of ROS generation during the contact process, we investigated the production of ROS on the SiO_2 surface as a function of contact time. ROS was not produced when water vapor–solid contact did not occur (Fig. 1*D*). The concentration of ROS generated on the SiO_2 surface gradually increased during the first 50 min of contact, after which it stabilized at 0.15 mg/g, suggesting the reaction reached steady state. Correspondingly, the concentration of ROS in the exiting gas also increased with contact occurrence and then approached a constant value (*SI Appendix*, Fig. S5).

To exclude the effect of solid–solid contact caused by gas injection, we studied the FT-IR spectra of a flat SiO_2 substrate before and after contact with water vapor. As shown in *SI Appendix*, Fig. S6*A* weak peak is observed after contact around 2,850 cm^{-1}, which is attributed to the generation of H_2O_2. This result confirmed that contact between water vapor and SiO_2 causes the generation of H_2O_2. Additionally, the signal from hydroxyl radicals can be observed by using electron spin resonance spectroscopy (ESR) at the surface of SiO_2 after contact as shown in Fig. 1 *E* and *F*. Hydroxyl radicals were detected in the leaving gas by using its reaction with 3,3′,5,5′-tetramethylbenzidine (TMB) to produce a colored product (37). *SI Appendix*, Fig. S7 displays the typical yellow color of the end-product of TMB oxidized by hydroxyl radicals and thus confirms the existence of hydroxyl radicals in the leaving gas. These results indicate that the contact between water vapor and solid substrate causes the generation of reactive oxygen species including hydroxyl radicals in a hydrated form and H_2O_2.

ROS Originates from the Reaction between Water Vapor and Surface Hydroxyl Groups. To investigate the origin of the spontaneous generation of H_2O_2 at the water vapor–solid interface, we carried out a series of in situ FT-IR spectroscopy measurements during the contact between water vapor and SiO_2 nanoparticles. We used a typical FT-IR spectrum of commercial SiO_2 nanoparticles as a baseline (as shown in *SI Appendix*, Fig. S8) for the observation of the changes in SiO_2 surface groups during the contact process. Fig. 2 *A* and *B* show the two-dimensional (2D) time-resolved FT-IR spectra of the SiO_2 nanoparticles during their contact with water vapor generated from DI water and a 10 % NaCl solution, respectively. These two 2D time-resolved FT-IR spectra are similar, indicating the generation of reactive oxygen species caused by water vapor–solid contact even at the high ionic strength of the source water. This observation can be attributed to the lower ionic strength in water vapor generated by gas bubbling than that of source water. This is similar to what happens when surface water evaporates into vapor. Therefore, we believe that water vapor–solid contact might be a more likely source of atmospheric oxidation in the Archean Eon than liquid–solid contact.

As shown in Fig. 2*B*, the FT-IR spectrum shows an intensity decrease in the 3,000 to 3,600 cm^{-1} region and an increase at 3,747 cm^{-1}. These changes in the FT-IR spectrum occur only after water vapor is introduced into the sealed chamber (the part of Fig. 2 below the black dashed line in each panel). This result suggests that water vapor may be one of the reactants in the generation of reactive oxygen species during the contact process. To further confirm the participation of water vapor in this reaction, a time-resolved FT-IR measurement was carried out when the contact happened at 120 °C. The heated sealed chamber rules out the existence of condensed water at the SiO_2 surface. As shown in Fig. 2*C*, a similar FT-IR signal change can be observed compared with FT-IR spectra in Fig. 2 *A* and *B*. The spectral intensity at 3,740 cm^{-1} slightly decreases, which may be caused by the shorter residence time of water molecules on the solid surface at the higher temperature. Typically, the adsorption band in the 3,000 to 3,800 cm^{-1} region can be attributed to the O–H stretching vibrations and related to their degree of hydrogen bonding. The peak at 3,230 cm^{-1} corresponds to the O–H stretching vibrations with a high degree of hydrogen bonding (icelike water). The peak at 3,400 cm^{-1} represents the adsorbed molecular water (liquid water) on the SiO_2 surface. The peak at 3,740 cm^{-1} seems to arise from the isolated hydroxyl group on SiO_2 (free OH) with no hydrogen bonds (38). As shown in Fig. 2 *A*–*C*, the contact between water vapor and SiO_2 leads to fragmentation of the hydrogen-bonding network on the SiO_2 surface, which suggests that hydroxyl groups on the SiO_2 surface (Si–OH) participate in the reaction generating H_2O_2. To test our speculation, we observed the 2D time-resolved FT-IR spectra of the SiO_2 nanoparticles during their contact with water vapor at 600 °C (shown in Fig. 2*D*). At this temperature, the water vapor–solid contact did not cause significant changes in FT-IR absorption spectrum. Considering the dehydration of the SiO_2 surface, this result indicates hydrogen-bonded hydroxyl groups also act as a reactant for H_2O_2 generation. Therefore, we propose that H_2O_2 generation during water vapor–solid contact originates from a physicochemical reaction between water vapor and surface hydroxyl groups on SiO_2. In addition, this finding further confirms that the contact of water vapor with metal-oxide nanoparticles is independent of the crystal structure of the solid substrate (24). In other words, hydroxyl functional groups on the surface of silicate minerals in the early Earth's atmosphere can be involved in ROS generation.

The Use of Isotopic Labeling. Tracing the changes of functional groups on the SiO_2 surface during its contact with water vapor is important to confirm our conjecture and further understand the reaction mechanism of H_2O_2 generation at the gas–solid interface. However, the O–H stretching vibrational signals of water vapor molecules adsorbed on the SiO_2 surface overlap with the signals from the original Si–OH, with low degree hydrogen bonding in the FT-IR spectrum. This overlap interferes with the observation of the water vapor–SiO_2 contact process. To distinguish the evolution of water vapor molecules and Si–OH during the contact process, deuterated water is used to produce D_2O gas in contact with SiO_2. Fig. 3*A* shows a typical 2D time-resolved FT-IR spectrum captured at the initial stage of the contact that occurred between D_2O vapor and commercial SiO_2. The increase of intensity of the band around 2,500 cm^{-1} indicates that O–D bonding is formed on the surface of SiO_2 nanoparticles during the gas–solid contact. In contrast, the intensity of the band at 3,000 to 3,600 cm^{-1} decreased during the contact process, which indicates hydrogen-bonded Si–OH groups decreased. We attribute this observation to two possible reasons: 1) the fragmentation of the O–H hydrogen bonding network during gas–solid contact and 2) the exchange of deuterium with hydroxyl groups on SiO_2.

Fig. 3*B* shows the corresponding FT-IR spectra captured at different contact durations. The change in the spectra with contact time shows that the structure of the hydrogen bonding network on the SiO_2 surface changes considerably during the first 30 min

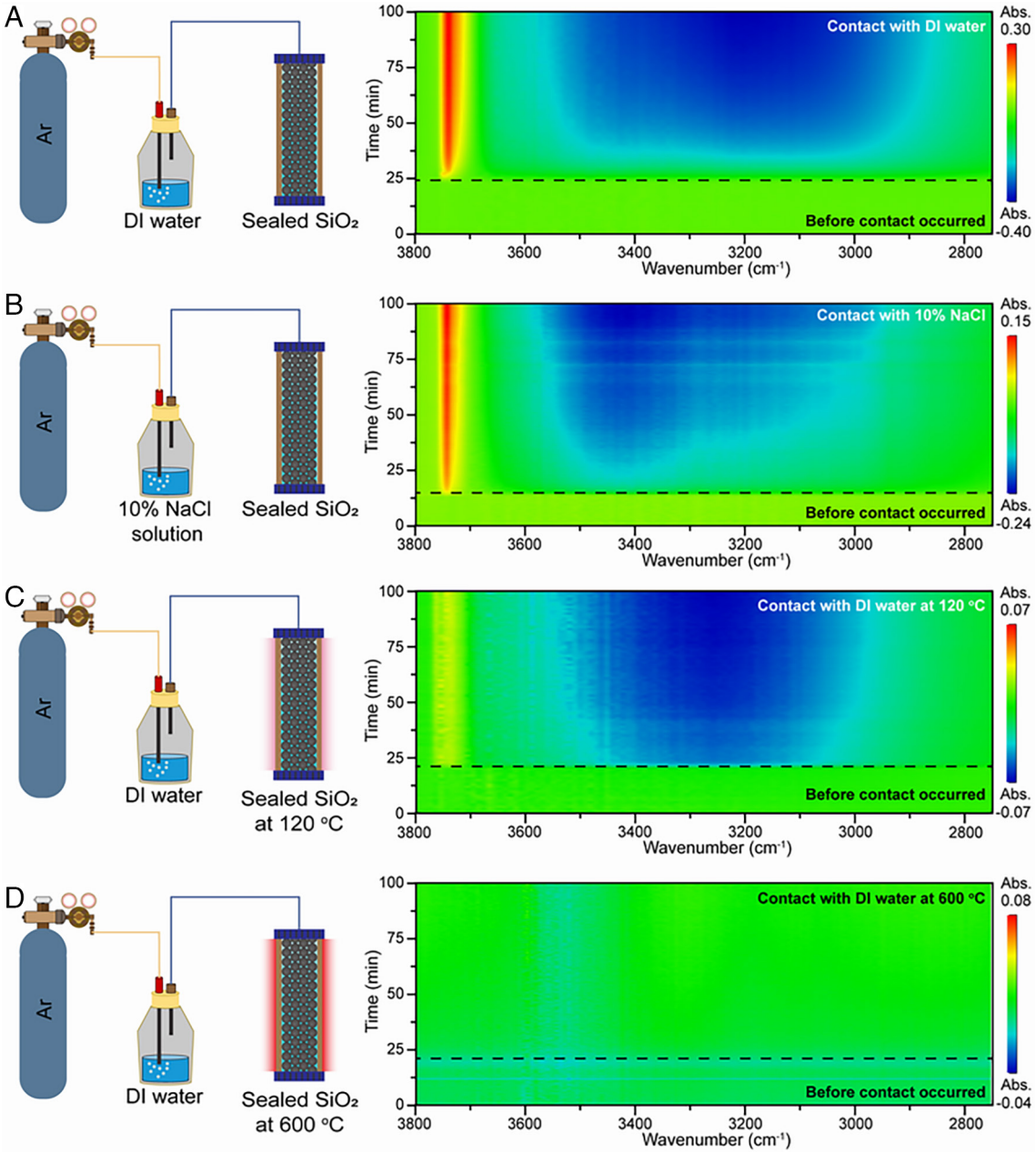

Fig. 2. The 2D time-resolved FT-IR spectra of SiO_2 during contact. (*A*) The 2D time-resolved FT-IR spectrum of the SiO_2 nanoparticles during their contact with water vapor generated from DI water at room temperature. (*B*) The 2D time-resolved FT-IR spectrum of the SiO_2 nanoparticles during their contact with water vapor generated from a 10% NaCl solution at room temperature. (*C*) The 2D time-resolved FT-IR spectrum of the SiO_2 nanoparticles during their contact with water vapor generated from DI water at 120 °C. (*D*) The corresponding 2D time-resolved FT-IR spectrum at 600 °C.

of contact and stabilized after 30 min. This trend is consistent with that of H_2O_2 generation on the surface of SiO_2 observed in Fig. 1*C*. These results reaffirm the relevance of structural changes in the OH hydrogen bonding network to the spontaneous generation of ROS on the SiO_2 surface during gas–solid contact. Additionally, a shoulder peak in the absorption band at 2,757 cm^{-1} is observed in Fig. 3 *B* and *C*, which can be attributed to isolated Si–OD groups. Importantly, no peak of isolated Si–OH groups at 3,740 cm^{-1} was detected. This result offers solid evidence that isolated Si–OH is one of the products of the physicochemical process caused by water vapor–solid contact, and the H atom in generated Si–OH originates from H_2O vapor.

To exclude the effect of the exchange of deuterium with hydroxyl groups on the above results, we place the SiO_2 in D_2O gas to saturate the exchange of hydrogen with deuterium in the hydroxyl groups on its surface. Then, we allowed the treated SiO_2 to contact the flowing D_2O vapor and observed the time-resolved FT-IR spectra of the SiO_2. As shown in Fig. 3 *D*–*F*, the intensity of the adsorption band in the 3,000 to 3,800 cm^{-1} region decreased, which suggests the fragmentation of the hydrogen bonding network on the SiO_2 surface that is not replaced by a deuterium-bonding network. Moreover, the band ranging from 2,000 to 2,500 cm^{-1} reveals that the deuterium-substituted hydrogen bonding network also breaks during the D_2O vapor–solid contact. The peak at 2,757 cm^{-1} is still observed, indicating that isolated Si–OD was generated during the above experiments. This result rules out the possibility that the peak formed from the exchange of deuterium with surface hydroxyl groups and further supports the contention that hydrogen from H_2O molecules may transfer to the SiO_2 surface during the H_2O vapor–solid contact.

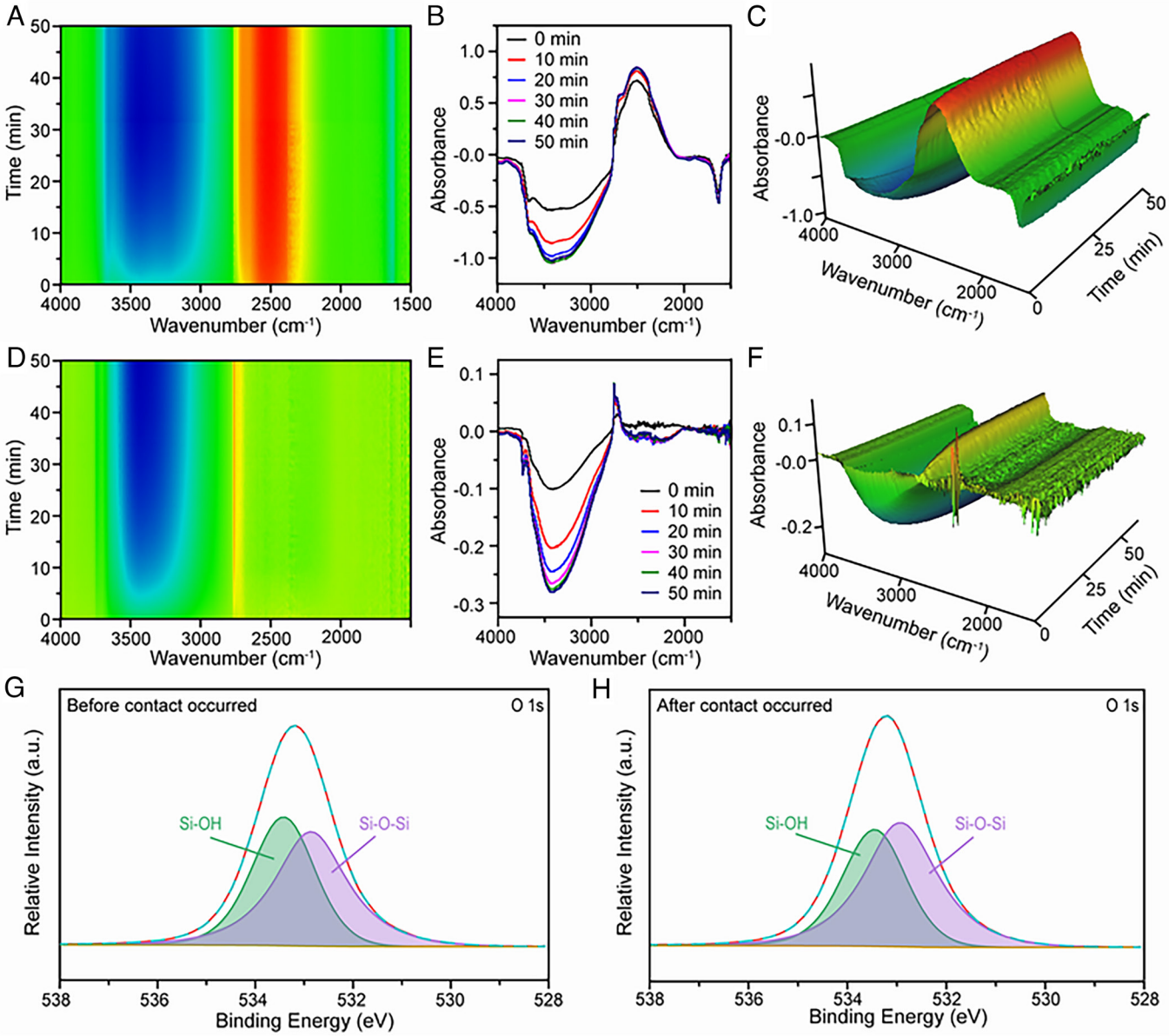

Fig. 3. FT-IR and XPS spectra of surface OH groups when contact occurred between SiO_2 nanoparticles and D_2O. (*A*) A typical 2D time-resolved FT-IR spectrum captured at the initial stage of the contact that occurred between D_2O vapor and commercial SiO_2. (*B*) The corresponding FT-IR spectrum in *A*. (*C*) The corresponding 3D time-resolved FT-IR spectrum in *A*. (*D*) A typical 2D time-resolved FT-IR spectrum during the contact that occurred between D_2O vapor and SiO_2 with hydroxyl groups after the exchange of hydrogen with deuterium. (*E*) The corresponding FT-IR spectrum in *D*. (*F*) The corresponding 3D time-resolved FT-IR spectrum in *D*. (*G*) The O 1S XPS spectra of SiO_2 before the contact occurred. (*H*) The corresponding O 1S XPS spectra after the contact occurred.

The X-ray photoelectron spectroscopy (XPS) spectra of the SiO_2 nanoparticles were measured before and after the water vapor–solid contact. As shown in Fig. 3 *G* and *H*, the atomic O 1s spectra are used to identify the type of surface oxygen species present in SiO_2. Two subpeaks at 533.4 eV (green) and 532.8 eV (purple) occurred, and they are assigned to the Si–OH and Si–O–Si bonds, respectively. After the contact between water vapor (H_2O) and SiO_2 occurred, the percentage of Si–OH in the O 1s peak decreases while that of Si–O–Si increases. This result suggests that the total density of Si–OH may decrease after the contact, which is in good agreement with the observation of the decrease of hydrogen-bonded OH in FT-IR spectra. Based on the FT-IR, XPS, and corresponding ROS concentration measurements, the change in the oxygen species on the SiO_2 surface reflects the generation of ROS, and this change originated from the fragmentation of the hydrogen-bonded OH network on the SiO_2 surface during the water vapor silicate contact and may be accompanied by the generation of Si–O–Si bonds.

Our previous work has indicated that, in the case of liquid-solid contact electrification, the generation of H_2O_2 from surface hydroxyl groups is accompanied by electron transfer (24). Contact electrification is important in providing the electron needed to drive the redox reaction on the surface. Therefore, we used Kelvin probe force microscopy (KPFM) to determine the surface charge density of the substrate before and after contact with water vapor (*SI Appendix*, Fig. S9). According to the earlier literature, we derive the potential into the charge density (39). The surface charge density of the substrate changed from 78.66 to −124.2 $\mu C\ m^{-2}$, which suggests that the substrate gained electrons in contact with water vapor. It is well known that contact electrification at the gas–solid interface is a pure electron-transfer process. Thus, the charge transfer measured in the process of the water vapor–solid contact electrification can be considered to be all from the contribution of electrons, as evidenced by the KPFM results after heat treatment (*SI Appendix*, Fig. S10). The number of transferred electrons is

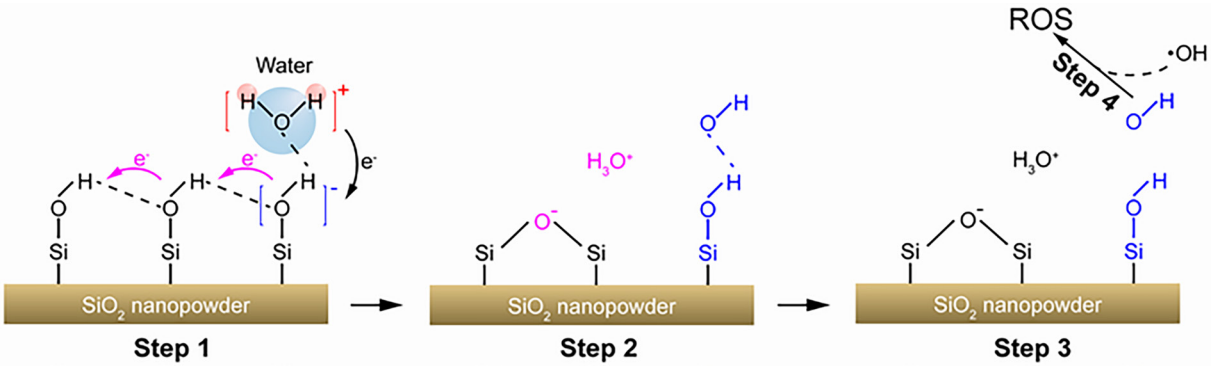

Fig. 4. Proposed mechanism for the ROS generation during contact electrification between water vapor and SiO_2.

one order of magnitude higher than that required for ROS generation. We believe that the electron transfer during the water vapor–solid contact electrification is sufficient to produce the amount of ROS that is observed. Additionally, this electron-transfer process demonstrates that the generation of ROS is not related to some ion migration process. Therefore, the contact electrification effect of water vapor with silicate minerals would produce ROS and is independent of ions that might have been present in the atmosphere and on the mineral surface.

Mechanism for Generation of ROS Based on Water Vapor–Silica Contact Electrification. Our experimental results and analysis revealed that when contact occurred between water vapor and SiO_2, isolated Si–OH group and hydroxyl radicals may be generated from the surface chemical reaction between water vapor and hydrogen-bonded hydroxyl groups on the SiO_2 surface. As shown in Fig. 4, we have constructed a possible reaction pathway using a structural unit consisting of three hydrogen-bonded hydroxyl groups on the surface of SiO_2. When contact occurred between water molecules and hydrogen-bonded hydroxyl groups, the electron cloud of the water molecule may overlap with that of the hydrogen-bonded hydroxyl group. Then, the electron may transfer from the water molecule to the surface of SiO_2, which is the so-called contact-electrification effect between water vapor and SiO_2. Thus, the adsorbed water molecules may be positively charged, while the hydrogen-bonding network on SiO_2 may be negatively charged (as shown in step 1 of Fig. 4). This behavior is also confirmed by the observation of a negatively charged current as shown in *SI Appendix*, Fig. S9. We speculate that as electrons transfer through the hydrogen-bonding network, the hydrogen bonds between the Si–OH break and dehydrate to produce hydrated hydrogen ions (hydronium cations) and negatively charged silyl ether oxygen bonds ($Si–O–Si^-$) as shown in step 2 of Fig. 4. After that, the active site where the water molecule overlaps with the hydroxyl group forms an intermediate structure Si–O – H–O, which further decomposes to form isolated Si–OH and hydroxyl radical (OH·) (step 3). Finally, recombination of OH· will generate H_2O_2 or complex with H_2O and H_3O^+ to generate hydrated hydroxyl radicals (step 4). We suggest that this mechanism explains why we can detect both H_2O_2 and hydroxyl radicals during the water vapor-solid contact.

Although the evolution of the hydrogen-bonding network structure on the SiO_2 surface in our proposed reaction mechanism is difficult to observe in situ, our results do indicate that the network structure composed of hydroxyl groups changes when water vapor comes into contact with the hydroxyl groups on the solid surface and is accompanied by the transfer of electrons and the generation of oxide species. Of course, the reaction pathway of this process has not been definitively established and deserves further investigation. In any case, the contact between water vapor and solid substrate and the corresponding evolution of surface hydrogen-boned Si–OH network structure plays an important role in the rise of reactive oxygen species, which may have contributed to the oxidation in the atmosphere of early Earth.

Conclusions

In summary, our results provide direct evidence for the spontaneous generation of ROS (H_2O_2, hydroxyl radicals, and hydrated hydroxyl radicals) at the SiO_2 surface from the reaction between hydrogen-bonded hydroxyl groups and water vapor. These observations give a new perspective on water vapor–silicate contact electrification and offer a possible reaction pathway for ROS generation at gas–solid interface. This reaction pathway offers a possible additional contribution to the rise of reactive oxygen species in the Archean Eon and enhances our understanding of the evolution of surface hydrogen bonding networks on silicate surfaces.

Materials and Methods

Materials. Unless otherwise stated, SiO_2 nanoparticles (200 to 300 nm, Shanghai Aladdin Bio-Chem Technology Co., Ltd., China), PTO dihydrate (99.99%, Sigma-Aldrich, USA), H_2O_2 standard solution (1,000 μg/mL, Beijing Northern Weiye Metrology Research Institute, China), anhydrous dimethyl sulfoxide (99.99%, Sigma-Aldrich, USA), (3,3′,5,5′-TMB, Sigma-Aldrich, USA), NaCl (AR, Sinopharm Chemical Reagent Co., Ltd., China), DI water (Merck Millipore, USA), deuterated water (D_2O, Sigma-Aldrich, USA), and argon (99.999%, Wuhan Iron and Steel Group Gas Co., Ltd., China) were used in experiments. Fourier transform infrared spectroscopy (Nicolet iS50, Thermo, USA) and in situ sealed reaction chamber (Harrick Scientific Products, Inc.) were used in experiments.

Quantitative Characterization of ROS. First, 0.15 g SiO_2 nanoparticles were filled into the sealed in situ reaction chamber, which has an integral inlet and an outlet. Argon was controlled at 0.15 MPa and passed through the safety bottle and wetted with DI water before entering the sealed reaction chamber. Then, a glass vial containing 1 mL of DI water was used to treat the exhaust gas in the sealed chamber, into which the ROS in the gas was dissolved. The entire process lasted 90 min. The exhaust gas without the addition of SiO_2 nanoparticles was treated under the same conditions and served as the experimental control group.

In addition, in order to quantitatively observe the remaining ROS on the surface of SiO_2 nanoparticles in relation to the reaction time, 0.15 g SiO_2 powder was packed into a sealed chamber, and 0.1 g samples were removed and dispersed into 1 mL of DI water at each certain reaction time (0, 10, 20…80, 90, and 100 min, total 11 samples). The first two groups of samples without argon were the experimental control group. The suspension was centrifuged (8,000 rpm for 10 min) to extract the upper clear layer for subsequent detection.

According to the literature, the chromogenic reaction of ROS with titanium salts is considered a reliable protocol for the accurate quantification of H_2O_2

concentration. H_2O_2 solutions of 0, 1, 2, and 3 mg L^{-1} were prepared using a H_2O_2 standard solution and were mixed with 0.1 M PTO aqueous solution in equal volume. In addition, 0.5 mL of samples were mixed with 0.1 M PTO aqueous solution in equal volume, and its absorbance at 400 nm was detected by a 96-well immuno plate (100 μL per well) and Microplate Reader.

Qualitative Characterization of Hydroxyl Radicals. As described above, 0.15 g of SiO_2 powder was loaded into a sealed chamber and 0.15 MPa moist argon gas was passed through. Then, 2 mL of a 10 μg/mL TMB/DMSO solution was used to absorb the exhaust gas. In addition, the SiO_2 nanoparticles before and after the reaction were characterized by ESR against hydroxyl radicals, and the trapping agent was DMPO.

2D Time-Resolved FT-IR Spectra Characterization. To investigate the effect of solid surface hydroxyl or adsorbed water on the whole process, the temperature of the sealed chamber was raised to 120 °C and 600 °C, respectively. In addition, the first 20 min of time-resolved FT-IR spectra were the control group with argon off (0.15 MPa). The argon gas is wetted with DI water. After 20 min, argon was turned on and changes in the material surface groups were recorded continuously (once a minute). The whole process continued for 100 min.

To test the effect of ionic strength in the carrier gas on the reaction, the DI water was replaced with a 10% sodium chloride solution. The chamber temperature was room temperature (25 °C). In addition, the subsequent reaction process was unchanged, with argon turned off for the first 20 min, then turned on and continued for 80 min.

The DI water was replaced by deuterium water to further trace the process of SiO_2 surface functional group change by introducing isotopes. The chamber temperature was room temperature (25 °C). Unreacted SiO_2 was used as the blank group, and argon was used as the carrier gas. The whole process was recorded with a FT-IR spectrometer, once a minute, for 50 min.

Then, 0.5 g SiO_2 nanoparticles were placed flat in a D_2O vapor environment to achieve the interchange of solid surface hydroxyl groups with deuterium hydroxyl groups and left to rest for 60 min. Subsequently, 0.15 g of the treated powder was taken into a sealed chamber with a reaction temperature of 25 °C and a carrier gas of argon (wetted with D_2O). The whole process was recorded with a FT-IR spectrometer, once a minute, for 50 min.

Effects of Surface Hydroxyl Groups on ROS Generation. XPS was used to characterize the surface group changes of the SiO_2 nanoparticles before and after the flow of water vapor. XPS was performed on a multifunctional imaging electron spectrometer (ESCALAB 250XI, Thermo) using monochromatized Al Ka radiation (1486.6 eV). The potential changes of the glass substrate surface before and after the flow of water vapor were obtained by KPFM experiments. Experiments were performed on a commercial AFM instrument (Multimode eight Bruker, USA). NSC 18 (MikroMash, USA; Au coated; tip radius: 25 nm; spring constant: 2.8 N m^{-1}) was used as the conductive tip here.

Data, Materials, and Software Availability. All data are included in the manuscript and *SI Appendix*. And the publicly available link: https://github.com/YuXia19/Yu-data (40).

ACKNOWLEDGMENTS. We thank Kurt W. Kolasinski and Peter R. Buseck for critically reading a first draft of this manuscript. This work was financially supported in part by grants from the National Key Research and Development Program of China (2020YFA0907400), and the National Nature Science Foundation of China (22193051, 22193052, and 22136006). R.N.Z. acknowledges the support from the US Air Force Office of Scientific Research through the Multidisciplinary University Research Initiative program (AFOSR FA9550-21-1-0170).

Author affiliations: [a]State Key Laboratory of Precision Blasting, Jianghan University, Wuhan 430056, China; [b]Hubei Key Laboratory of Environmental and Health Effects of Persistent Toxic Substances, Jianghan University, Wuhan 430056, China; [c]Department of Chemistry, Stanford University, Stanford, CA 94305; [d]School of Physics and Technology, Wuhan University, Wuhan 430072, China; and [e]State Key Laboratory of Environmental Chemistry and Ecotoxicology, Research Center for Eco-Environmental Sciences, Chinese Academy of Sciences, Beijing 10085, China

1. M. Tang, D. Cziczo, V. Grassian, Interactions of water with mineral dust aerosol: Water adsorption, hygroscopicity, cloud condensation, and ice nucleation. *Chem. Rev.* **116**, 4205–4259 (2016).
2. H. Sies, Role of metabolic H_2O_2 generation. *J. Bio. Chem.* **289**, 8735–8741 (2014).
3. N. Smironoff, D. Arnaud, Hydrogen peroxide metabolism and functions in plants. *New Phytologist.* **221**, 1197–1214 (2019).
4. J. Bates *et al.*, Review of acellular assays of ambient particulate matter oxidative potential: Methods and relationships with composition, sources, and health effects. *Environ. Sci. Technol.* **53**, 4003–4019 (2019).
5. R. Ball, J. Brindley, The power without the glory: Multiple roles of hydrogen peroxide in mediating the origin of life. *Astrobiology* **19**, 675–684 (2019).
6. R. E. Blankenship, H. Hartman, The origin and evolution of oxygenic photosynthesis. *Trends Biochem. Sci.* **23**, 94–97 (1998).
7. C. P. McKay, H. Hartman, Hydrogen peroxide and the evolution of oxygenic photosynthesis. *Orig. Life Evol. Biosph.* **21**, 157–163 (1991).
8. H. He *et al.*, An abiotic source of Archean hydrogen peroxide and oxygen that pre-dates oxygenic photosynthesis. *Nat. Commun.* **12**, 6611 (2021).
9. C. M. Ostrander *et al.*, Earth's first redox revolution. *Annu. Rev. Earth Planet. Sci.* **49**, 337–366 (2021).
10. H. He *et al.*, A mineral-based origin of Earth's initial hydrogen peroxide and molecular oxygen. *Proc. Natl. Acad. Sci. U.S.A.* **120**, e2221984120 (2023).
11. J. Xiong, W. M. Fischer, K. Inoue, M. Nakahara, C. E. Bauer, Molecular evidence for the early evolution of photosynthesis. *Science* **289**, 1724–1730 (2000).
12. D. C. Catling, K. J. Zahnle, The archean atmosphere. *Sci. Adv.* **6**, eaax1420 (2020).
13. I. G. Draganić, E. Bjergbakke, Z. D. Draganić, K. Sehested, Decomposition of ocean waters by potassium-40 radiation 3800 Ma ago as a source of oxygen and oxidizing species. *Precambrian Res.* **52**, 337–345 (1991).
14. J. F. Kasting, J. B. Pollack, D. Crisp, Effects of high CO_2 levels on surface temperature and atmospheric oxidation state of the early Earth. *J. Atmos. Chem.* **1**, 403–4428 (1984).
15. J. Haqq-Misra, J. F. Kasting, S. Lee, Availability of O_2 and H_2O_2 on pre-photosynthetic Earth. *Astrobiology* **11**, 293–302 (2011).
16. E. Pecoits *et al.*, Atmospheric hydrogen peroxide and eoarchean iron formations. *Geobiology* **13**, 1–14 (2015).
17. J. K. Lee *et al.*, Spontaneous generation of hydrogen peroxide from aqueous microdroplets. *Proc. Natl. Acad. Sci. U.S.A.* **116**, 19294–19298 (2019).
18. J. K. Lee *et al.*, Condensing water vapor to droplets generates hydrogen peroxide. *Proc. Natl. Acad. Sci. U.S.A.* **117**, 30934–30941 (2020).
19. M. T. Dulay *et al.*, Spraying small water droplets acts as a bactericide. *QRB Discovery* **1**, e3 (2020).
20. M. T. Dulay *et al.*, Effect of relative humidity on hydrogen peroxide production in water droplets. *QRB Discovery* **2**, e8 (2021).
21. T. Kakeshpour, B. Metaferia, R. N. Zare, A. Bax, Quantitative detection of hydrogen peroxide in rain, air, exhaled breath, and biological fluids by NMR spectroscopy. *Proc. Natl. Acad. Sci. U.S.A.* **119**, e2121542119 (2022).
22. D. Xing *et al.*, Capture of hydroxyl radicals by hydronium cations in water microdroplets. *Angew. Chem. Int. Ed.* **61**, e202207587 (2022).
23. M. A. Mehrgardi, M. Mofidfar, R. N. Zare, Sprayed water microdroplets are able to generate hydrogen peroxide spontaneously. *J. Am. Chem. Soc.* **144**, 7606–7609 (2022).
24. B. Chen *et al.*, Water-solid contact electrification causes hydrogen peroxide production from hydroxyl radical recombination in sprayed microdroplets. *Proc. Natl. Acad. Sci. U.S.A.* **119**, e2209056119 (2022).
25. Y. Abe, Physical state of the very early Earth. *Lithos* **30**, 223–235 (1993).
26. P. R. Salve, A. Maurya, S. R. Wate, S. Devotta, Chemical composition of major ions in rainwater. *Bull. Environ. Contam. Toxicol.* **80**, 242–246 (2008).
27. S. Lin, L. Zhu, Z. Tang, Z. L. Wang, Spin-selected electron transfer in liquid-solid contact electrification. *Nat. Commun.* **13**, 5230 (2022).
28. S. Lin, L. Xu, A. C. Wang, Z. L. Wang, Quantifying electron-transfer in liquid-solid contact electrification and the formation of electric double layer. *Nat. Commun.* **11**, 399 (2020).
29. Z. Tang, S. Lin, Z. L. Wang, Effect of surface pre-charging and electric field on the contact electrification between liquid and solid. *J. Phys. Chem. C* **126**, 8897–8905 (2022).
30. Z. L. Wang, A. C. Wang, On the origin of contact-electrification. *Mater. Today* **30**, 34–51 (2019).
31. W. Zhang, Y. Shi, Y. Li, X. Chen, H. Shen, A review: Contact electrification on special interfaces. *Front. Mater.* **9**, 909746 (2022).
32. J. S. Méndez Harper *et al.*, Electrification of sand on titan and its influence on sediment transport. *Nat. Geosci.* **10**, 260–265 (2017).
33. T. W. Lyons, C. T. Reinhard, N. J. Planavsky, The rise of oxygen in Earth's early ocean and atmosphere. *Nature* **506**, 307–315 (2014).
34. C. Sagan, G. Mullen, Earth and mars: Evolution of atmospheres and surface temperatures. *Science* **177**, 52–56 (1972).
35. S. Boggs, *Principles of Sedimentology and Stratigraphy* (Pearson Prentice Hall, Upper Saddle River, NJ, ed. 4th, 2006), pp. 119–135.
36. D. Xing *et al.*, Capture of hydroxyl radicals by hydronium cations in water microdroplets. *Angew. Chem. Int. Ed.* **61**, e202207587 (2022).
37. X. Ma *et al.*, A universal multicolor immunosensor for semiquantitative visual detection of biomarkers with the naked eyes. *Biosens. Bioelectron.* **87**, 122–128 (2017).
38. D. B. Asay, S. H. Kim, Evolution of the adsorbed water layer structure on silicon oxide at room temperature. *J. Phys. Chem. B* **109**, 16760–16763 (2005).
39. S. Lin, L. Xu, A. C. Wang, Z. L. Wang, Quantifying electron-transfer in liquid-solid contact electrification and the formation of electric double-layer. *Nat. Commun.* **11**, 399 (2020).
40. X. Yu, Yu's data. Github. https://github.com/YuXia19/Yu-data. Deposited 25 June 2023.